SDC
OPEN

HISTOLOGY OF GEOGRAPHIC ATROPHY SECONDARY TO AGE-RELATED MACULAR DEGENERATION

A Multilayer Approach

MIAOLING LI, MD, PHD,*† CARRIE HUISINGH, MSPH,* JEFFREY MESSINGER, DC,* ROSA DOLZ-MARCO, MD, PHD,‡§¶ DANIELA FERRARA, MD, PHD,** K. BAILEY FREUND, MD,‡§†† CHRISTINE A. CURCIO, PHD*

Purpose: To systematically characterize histologic features of multiple chorioretinal layers in eyes with geographic atrophy, or complete retinal pigment epithelium (RPE) and outer retinal atrophy, secondary to age-related macular degeneration, including Henle fiber layer and outer nuclear layer; and to compare these changes to those in the underlying RPE-Bruch membrane—choriocapillaris complex and associated extracellular deposits.

Methods: Geographic atrophy was delimited by the external limiting membrane (ELM) descent towards Bruch membrane. In 13 eyes, histologic phenotypes and/or thicknesses of Henle fiber layer, outer nuclear layer, underlying supporting tissues, and extracellular deposits at four defined locations on the non-atrophic and atrophic sides of the ELM descent were assessed and compared across other tissue layers, with generalized estimating equations and logit models.

Results: On the non-atrophic side of the ELM descent, distinct Henle fiber layer and outer nuclear layer became dyslaminated, cone photoreceptor inner segment myoids shortened, photoreceptor nuclei and mitochondria translocated inward, and RPE was dysmorphic. On the atrophic side of the ELM descent, all measures of photoreceptor health declined to zero. Henle fiber layer/outer nuclear layer thickness halved, and only Müller cells remained, in the absence of photoreceptors. Sub-RPE deposits remained, Bruch membrane thinned, and choriocapillaris density decreased.

Conclusion: The ELM descent sharply delimits an area of marked gliosis and near-total photoreceptor depletion clinically defined as Geographic atrophy (or outer retinal atrophy), indicating severe and potentially irreversible tissue damage. Degeneration of supporting tissues across this boundary is gradual, consistent with steady age-related change and suggesting that RPE and Müller cells subsequently respond to a threshold of stress. Novel clinical trial endpoints should be sought at age-related macular degeneration stages before intense gliosis and thick deposits impede therapeutic intervention.

RETINA 38:1937–1953, 2018

Age-related macular degeneration (AMD) is a major cause of vision loss worldwide.[1] While neovascular AMD can be clinically managed with anti-vascular endothelial growth factor therapy,[2] geographic atrophy (GA), the end stage of non-neovascular AMD, lacks an effective treatment or prevention.[3] Geographic atrophy is characterized by a degeneration of photoreceptors and their supporting tissues (retinal pigment epithelium [RPE], Bruch membrane [BrM] and choriocapillaris [ChC]), in the setting of characteristic extracellular deposits. Geographic atrophy enlargement is a clinical trial endpoint accepted by the U.S. Food and Drug Administration for use in treatment trials for non-neovascular AMD.[4,5] How GA is diagnosed and measured has implications for generating scientific hypotheses, designing trials, interpreting outcomes, and counseling patients.[6] Remarkably, organized retinal tissue layers can be appreciated in clinical optical coherence tomography (OCT).[7–9] An international expert group is establishing consensus and redefining atrophy based upon OCT-anchored multimodal imaging.[3,10] In this new nomenclature, GA is

an example of complete RPE and outer retinal atrophy (cRORA).

Optical coherence tomography metrics for GA identification and enlargement focus on RPE absence, as revealed by the hypertransmission sign, that is, more light reaching sub-RPE structures such as the choroid. However, overlying photoreceptors are also readily visible in OCT, and anatomical bases of photoreceptor-attributable reflective bands have been proposed. Bands have been named external limiting membrane (ELM), ellipsoid zone (EZ), and interdigitation zone,[11,12] the anatomical Henle fiber layer (HFL) and outer nuclear layer (ONL) have been separated within the single hyporeflective ONL,[13,14] and hyperreflective basal laminar deposit (BLamD) that persists across the atrophic zone is distinguishable from the outer plexiform layer (OPL).[15,16]

According to S.H. Sarks, a curved line formed by the ELM descending towards BrM is the boundary of photoreceptor and RPE atrophy[17] (Figure 1), with both cell types degenerating near the atrophic area, in which they disappear. The ELM is a series of junctional complexes between photoreceptors and Müller glia. The curved ELM descent signifies gliosis of Müller cells[18] in the setting of extreme photoreceptor degeneration. These normally vertical support cells extend horizontally and scroll in concert with the expanding area of RPE atrophy, while also expressing glial fibrillary acidic protein,[19,20] thus indicating severe and potentially irreversible tissue damage. In contrast to the RPE layer, which ends raggedly, the ELM descent is a precise border to delimit the GA area in a manner that is also useful for analyzing disease progression.[9] In eyes with GA, we recently determined the frequency of RPE morphologic phenotypes and measured the thickness of RPE and BLamD at four standard locations, two on either side (non-atrophic and atrophic) of the lesion area delimited by the ELM descent.[9] We thus quantified and suggested as possible OCT biomarkers a progressive RPE dysmorphia and thickening of the RPE-BLamD layers toward this boundary.

By similarly analyzing other retinal and choroidal layers in a multilayered approach, we can address long-standing questions about the initial site of damage in AMD, of importance for informing therapeutic strategies. The vertically organized and tightly integrated physiologic unit of photoreceptors, Müller cells, RPE, and ChC can be productively considered as the outer retinal neurovascular unit.[21] This concept, developed originally for brain and then inner retina,[22,23] comprises micro-vessels, neurons, glia, pericytes, and extracellular matrix that couple blood flow to the metabolic demands of neurons. Age-related macular degeneration can be conceived as either a neurodegeneration or a disease of vascular/metabolic insufficiency, depending on the initial site of damage. Previous research showing lipid buildup in macular BrM throughout adulthood and leading to soft drusen,[13,24] and ChC decline in aging,[25–29] supports a vascular model of AMD initiation. This hypothesis could be tested further by comparing layers of the neurovascular unit in individual eyes with GA, which has not been attempted to date.

To generate further insights on GA pathogenesis, to inform the interpretation of GA seen by OCT-based multimodal imaging, and to contextualize our forthcoming clinicopathologic correlation studies, the purposes of this current work are 2-fold: 1) to provide a histologic basis and potential biomarkers for reflective bands encompassing photoreceptors and Müller cells in OCT imaging in eyes with GA, thus including the HFL and ONL; 2) to develop a timeline of disease progression by quantifying changes in these layers as a function of distance from the ELM descent, in non-atrophic and atrophic areas, and in relation to the underlying supporting tissues and extracellular deposits (subretinal drusenoid deposits [SDDs], BLamD, and drusen).[9] We use high-resolution and comprehensive cross-sectional histology. This format both emulates OCT[30] and discloses all the biologically distinct layers of pathology in the RPE-basal lamina-BrM (RBB) complex. Our results highlight an active role

From the *Department of Ophthalmology, School of Medicine, University of Alabama at Birmingham, Birmingham, Alabama; †State Key Laboratory of Ophthalmology, Zhongshan Ophthalmic Center, Sun Yat-sen University, Guangzhou, China; ‡Vitreous Retina Macula Consultants of New York, New York; §LuEsther T Mertz Retinal Research Center, Manhattan Eye, Ear and Throat Hospital, New York, New York; ¶Oftalvist Clinic, Valencia, Spain; **Genentech, South San Francisco, California; and ††Department of Ophthalmology, New York University School of Medicine, New York, New York.

Supported by Hoffman LaRoche, the Macula Foundation, Inc, and unrestricted funds to the Department of Ophthalmology from Research to Prevent Blindness, Inc, and EyeSight Foundation of Alabama. Project MACULA tissue acquisition and website construction was supported by NIH grants EY06109 (C.A.C.), International Retinal Research Foundation, Edward N. and Della L. Thome Foundation, Arnold and Mabel Beckman Initiative for Macular Research, and NEI Core grant P30 EY003039.

Supplemental digital content is available for this article. Direct URL citations appear in the printed text and are provided in the HTML and PDF versions of this article on the journal's Web site (www.retinajournal.com).

Reprint requests: Christine A. Curcio, PhD, Department of Ophthalmology, EyeSight Foundation of Alabama Vision Research Laboratories, University of Alabama School of Medicine, 1670 University Boulevard Room 360, Birmingham, AL 35294-0099; e-mail: curcio@uab.edu

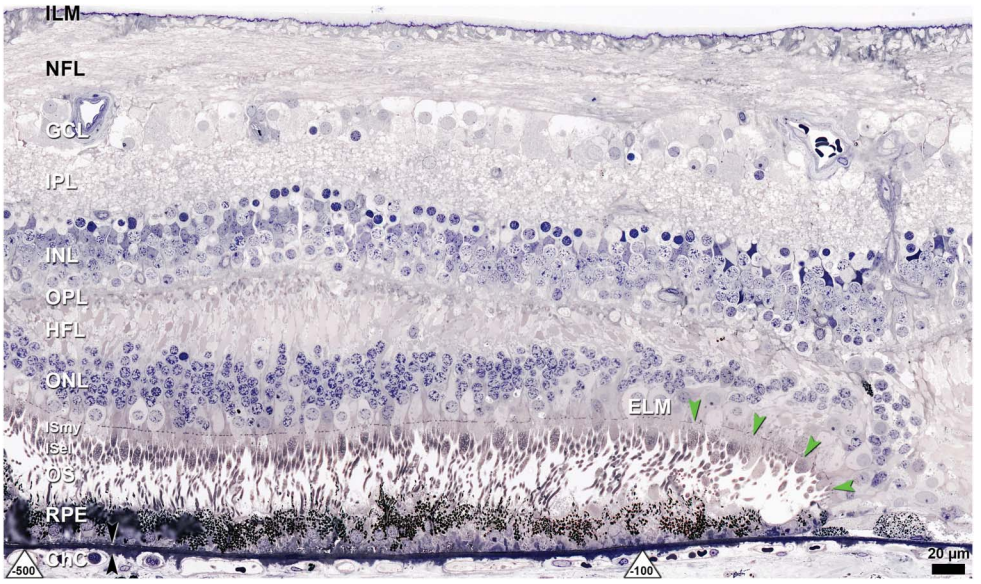

Fig. 1. External limiting membrane descent in an eye with geographic atrophy. ELM, external limiting membrane (green arrowheads); ILM, inner limiting membrane; NFL, nerve fiber layer; GCL, ganglion cell layer; IPL, inner plexiform layer; INL, inner nuclear layer; ISmy, inner segment myoid; ISel, inner segment ellipsoid; black arrowheads, Bruch membrane. The ELM descent is a curved line,[9,39] and ONL subsides in parallel with it. The distances of −100 and −500 μm to the ELM descent (white triangles) represent assessment locations. Eighty-seven-year-old white man.

of Müller glia in neuroprotection and clearing, different time courses of degeneration in outer retina vs. supporting tissues, and the potential utility of the ELM descent as an OCT landmark.

Methods

Compliance

Studies were approved by institutional review at the University of Alabama at Birmingham and adhered to the Tenets of the Declaration of Helsinki.

Tissue Source and Preparation

Tissue images were drawn from the Project MACULA website of AMD histopathology (http://www.projectmacula), created from short post-mortem (<6 hours) eyes of donors to the Alabama Eye Bank. Eyes were post-fixed in paraphenylenediamine, prepared for submicrometer epoxy sections, and stained with toluidine blue. Through histopathologic examination, eyes with GA were identified by the absence of a continuous RPE layer for at least >250 μm, in the presence of basal linear deposit or drusen and in the absence of evidence of neovascularization. For each eye, one section through the foveal rod-free zone (Central) and another in the rod-dominant perifovea at 2 mm superior to the foveal center (Superior) was analyzed. Sections were scanned using a 60× oil-immersion objective (numerical aperture = 1.4), using a microscope with a robotic stage and slide scanning software (Olympus VSI 120; CellSens; Olympus, Center Valley, PA). Images were viewed on a monitor at 1240X. For figures, images were adjusted for exposure, contrast, and background color correction (Photoshop CS6; Adobe Systems, San Jose, CA).

Cellular and Laminar Phenotypes

We used previously published phenotypes to characterize the RPE and extracellular deposits in this work.[9] Phenotypes for other layers will be newly described in the Results. As reviewed,[31] RPE morphology was surveyed histologically in 52 advanced AMD eyes, and linked to reflective OCT features in 6 eyes.[32–34] Phenotypes ranged from non-uniform (normal aging) to absent with and without BLamD and included sloughed (rounded, in the subretinal space), intraretinal (internal to the ELM), vitelliform (dispersed RPE organelles mixed with outer segments), dissociated (isolated nucleated cells in atrophic areas), and subducted (in the sub-RPE-basal laminar space).

Regarding extracellular deposits, BLinD was recognized as a layer of grayish-pink flocculent material in the sub-RPE compartment continuous with soft drusen, that is, mounds of the same material.[35] Both were differentiable from overlying BLamD and underlying inner collagenous, elastic, and outer collagenous layers of BrM, which appeared as a single dark blue line. Basal laminar deposit is a stereotypically structured thick layer of basement membrane material between the RPE plasma membrane and the native basal lamina. Basal laminar deposit is scalloped and light blue near the RPE (late form) and dark blue palisades (early form) near BrM.[15,36,37] Subretinal drusenoid deposit was a pale-staining flocculent material with finely particulate inclusions, located between the apical surface

of the RPE and photoreceptor outer segments.[35] In detached specimens, SDD adhere to either RPE or photoreceptors; measured thicknesses in histology thus underestimate thicknesses in vivo.

Measurements

We measured the total distance between the OPL and ELM, and thicknesses of the HFL and ONL as proportions of this total. Where the ELM was absent, RPE was also absent, and thus OPL-ELM thickness was measured from OPL to the inner surface of the BLamD that persisted after loss of RPE. We measured inner segment myoid (ISmy) as a metric of cone degeneration, because it shrinks as mitochondria from the ellipsoid retract towards the cell body,[8] and because continuity of ISmy with photoreceptor cell bodies internal to the ELM could be verified. Inner segment ellipsoids and outer segments can become artifactually curved and compacted, like a stepped-on lawn, even in attached retinas, and were not measured. We used previously reported RPE and BLamD thicknesses.[9] The thickness of RPE-basal laminar (sub-RPE-BL) space[30] including all contents (drusen material and cells) was measured. Bruch membrane thickness was measured between intercapillary pillars only. Finally, we measured ChC density, the total apposition of ChC to BrM[29] within a 200-μm segment, as a metric of capillary exchange capacity and expressed as a proportion between 0 and 1.

Sampling Strategy

We recorded phenotypes and measured layers at four defined locations (±100/500 μm) along BrM, relative to the ELM descent, as described.[9] Negative distances (−500 and −100 μm) represent locations on the non-atrophic side of the ELM descent adjacent to the GA lesion. Positive distances (+100 and +500 μm) represent locations on the atrophic side, within the GA lesion. Tables and descriptions follow a discretized progression timeline from left (non-atrophic) to right (atrophic). In attached specimens, photoreceptor and RPE layers are directly apposed. In general, non-atrophic retina, even in eyes recovered quickly after death, often detached from the RPE, while atrophic retina remained attached to BrM. In detached specimens, we matched the photoreceptor layer to underlying RPE by determining overall shrinkage of retina versus intact RPE-choroid-sclera, using anchor points (e.g., peripapillary BrM), and features that could be matched across the detachment.

In total, we analyzed 13 eyes of 12 donors with a histologic diagnosis of GA (8 women, 4 men,

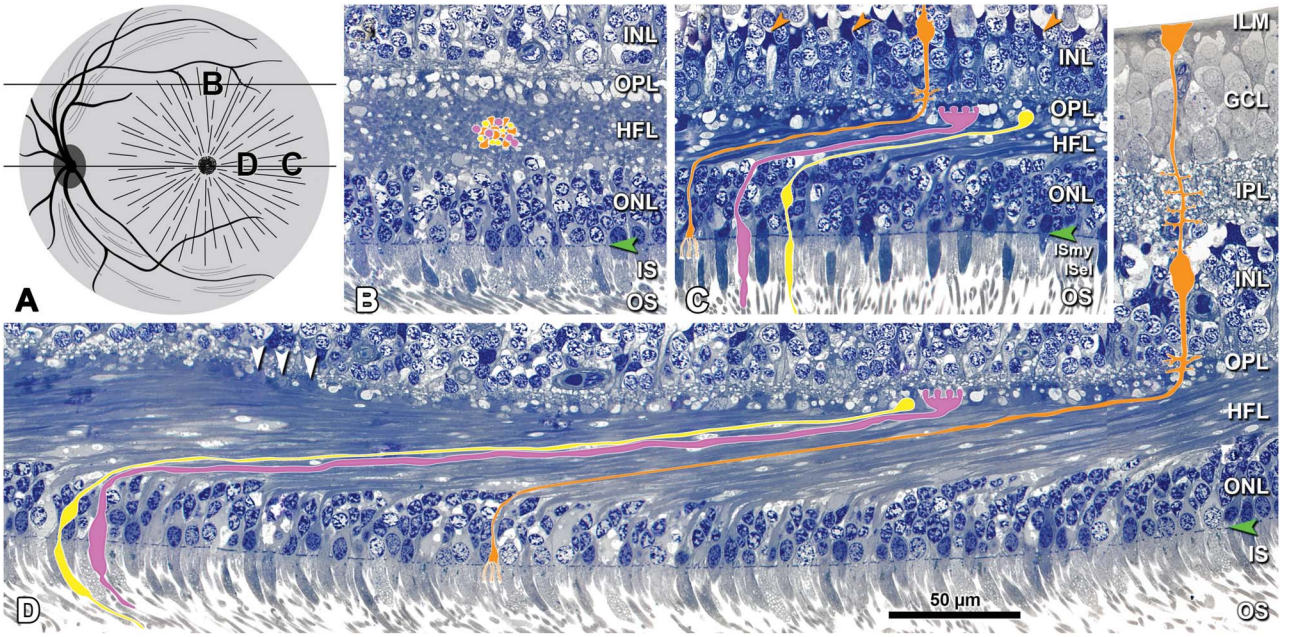

Fig. 2. Geometry of Henle fiber layer in a normal macula. INL, inner nuclear layer; external limiting membrane, green arrowheads; IS, inner segment; ISmy, inner segment myoid; ISel, inner segment ellipsoid; OS, outer segment. Bar in (**D**) applies to all panels. Eighty-year-old woman. **A.** An *en face* view of henle fibers shows their radial dispersion from the foveal center. **B–D.** Indicate the locations of sections in (**B**), (**C**) and (**D**). **B.** In the superior perifovea are cross-sections of rods (yellow dots), cones (pink dots) with Müller cells in between (orange dots). **C.** In the perifoveal area of the central section, henle fibers are longitudinally oriented but short. A Müller cell (orange), rod (yellow) and cone (pink) photoreceptor are shown. One fiber is 115-μm long (from ELM to outer surface of OPL). Müller cell bodies, orange arrowheads. **D.** Close to the fovea in the central section, henle fibers are longitudinally oriented and long. One fiber is 350-μm-long (from ELM to outer surface of OPL). Müller, orange; rod, yellow; cone, pink.

85.6 ± 4.9 years), 18 sections (13 Central, 5 Superior), 69 ELM descents, and 170 (N) assessment locations (36, 62, 47, and 25 at −500, −100, +100, and +500 μm, respectively). The number and pattern of assessment locations differed among eyes, because in some cases atrophic areas extended off section edges, were less than 1,000 μm wide, or did not extend into superior macula. Scanned histologic images were scaled for tissue units, centered, viewed on a monitor at magnifications up to 1900X, and annotated by a single trained observer (M.L.) with supervision (C.A.C.). Annotations were recorded in a custom database with drop-down menus (Filemaker; Adobe, San Jose, CA),[9,38,39] while digital sections were manipulated with FIJI (https://imagej.net/Fiji).

Statistics

Generalized estimating equations linear models were used to compare mean layer thicknesses, separately and in combination, especially between non-atrophic and atrophic areas. A generalized logit model was used to assess the relationship between RPE morphology, RBB thickness, BrM thickness, and ChC density with three levels of ONL health (i.e., ONL thickness >0, dyslaminated, ONL thickness = 0), where the term dyslamination refers to loss of a discrete HFL and ONL (see Results). The generalized logit assumes these categories are nominal (not ordered). Thickness >0 was used as the referent category. The model describes the log odds that a given RPE morphology will have an ONL status of 0 or dyslaminated instead of >0. Similar considerations apply to levels of RBB thickness, BrM thickness, and ChC density. A P-value <0.05 was considered statistically significant.

Results

At each assessment point we characterized pathology using a categorical system of cellular phenotypes.[9,39] Henle fiber layer, ONL, BrM and ChC phenotypes were newly defined for this study. We present data layer by layer from inner to outer, then compare the results across layers.

The HFL radiation is familiar to clinicians as the anatomical substrate of macular star. We describe its geometry using the nomenclature of Polyak.[40] This layer, unique to macula, contains the Henle fibers,[7,40,41] that is, cone and rod fibers (between cell bodies in the ONL and synaptic terminals in OPL) and

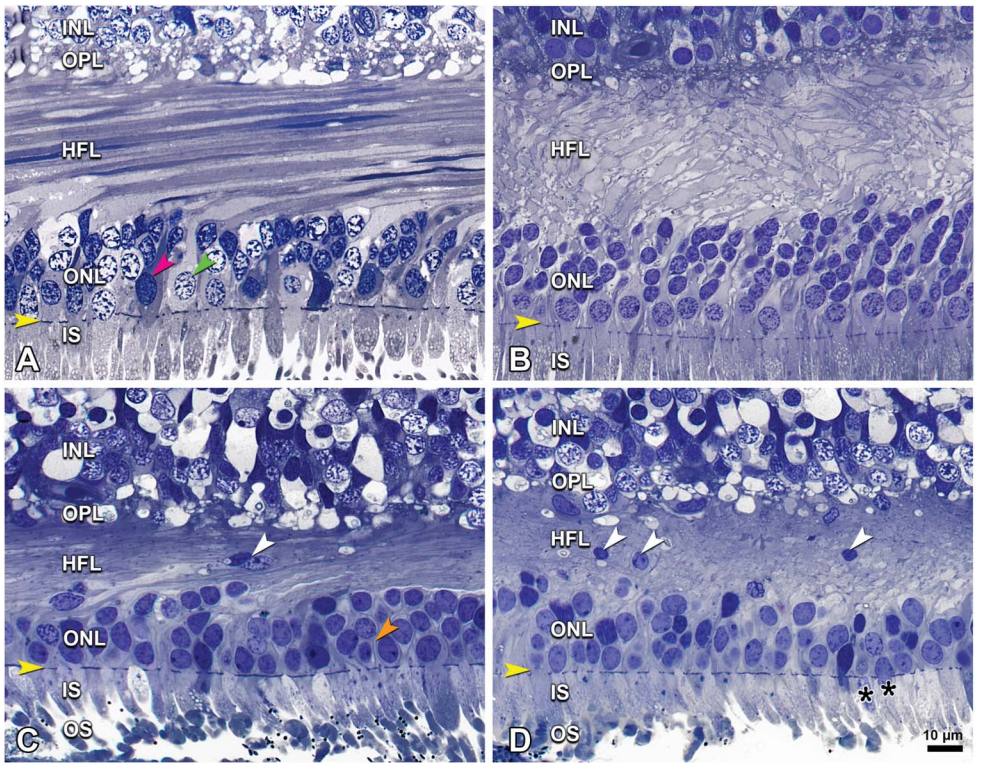

Fig. 3. Different presentations of the Henle fiber layer in eyes with geographic atrophy. INL, inner nuclear layer; external limiting membrane, yellow arrowheads; IS, inner segment; OS, outer segment. Bar in (**D**) applies to all panels. **A.** The ordered henle fibers in the central section are long and longitudinally oriented (1,400 μm to ELM descent, non-atrophic side), typical of normal retina but also a possible presentation in eyes with GA. Rod nucleus, pink arrowhead; cone nucleus, green arrowhead. Eighty-five-year-old woman. **B.** The henle fibers in the central section are disordered, having lost their longitudinal orientation (200 μm to ELM descent, non-atrophic side). Seventy-six-year-old woman. **C.** Ectopic photoreceptor nuclei (white arrowhead) in ordered HFL are seen at the central section (1,200 μm to ELM descent, non-atrophic side). Müller cell processes, orange arrowhead. Eighty-eight-year-old woman. **D.** The superior perifovea section of same eye as panel C, ectopic photoreceptor nuclei (white arrowheads) in disordered HFL are detected (900 μm to ELM descent, non-atrophic side). Photoreceptor nuclei ectopic to IS, black asterisks.

inner fibers of Müller glia (between the ELM and cell bodies in the inner nuclear layer) (Figure 2). In a normal aged macula, rods outnumber cones 6:1,[42] and cones and Müller cells may be equal in number.[43] In histological cross-sections, Henle fibers appear as longitudinal profiles that are long close to the fovea and shorter but still longitudinal in the perifovea (Figure 2, D and C).[7] In the superior perifovea, fibers appear as small circular cross-sections (Figure 2B). In eyes with GA, Henle fibers can remain ordered (Figure 3A), or become disordered, with or without ectopic photoreceptor nuclei (Figure 3, B–D) that leave the continuous ONL and cross into HFL (Figure 3, C and D).

Normal ONL is shown in Figure 4, A and B. Outer nuclear layer can be seen as thinned (Figures 4C, D and 5B) in comparison to thicker unremarkable ONL elsewhere in the same eye. Photoreceptor nuclei can retract inwardly from the ELM and towards the HFL as a group, while the boundary between HFL and ONL is still visible (see Figure 3B of Ref. 8). Retracted mitochondria move inwardly within cone inner segments toward the nucleus (see Figure 7 of Ref. 8). Frequently, the distinction between HFL and ONL was lost due to scattering of photoreceptor nuclei across the HFL (Figure 5), a phenomenon we called dyslamination. Dyslamination comprises ONL depopulation, inward migration of photoreceptor cell bodies across the HFL, and gliosis of interleaved Müller cell processes. Outer retinal tubulation and photoreceptor islands, if present, involve HFL and ONL.[44–46] The ONL can be absent with or without the presence of RPE (Figure 6), and ELM loss accompanies RPE loss. Notably, the HFL is visible even if the ONL is completely absent (Figure 6A) or contains only isolated cone photoreceptor bodies (Figure 6B). In these instances, the HFL is filled by Müller cells.

Outer retinal phenotypes and thicknesses are presented in Table 1. Ectopic photoreceptor nuclei in HFL (Figure 3, C and D, white arrowheads) are common in the non-atrophic area (48.4%–62.9% of locations), whereas ectopic nuclei in IS (Figure 3D, black asterisks) are infrequent (9.7%–11.4%). As the atrophic zone is approached, ordered HFL decreased from 57.1% to 16.0% of locations and abnormal HFL

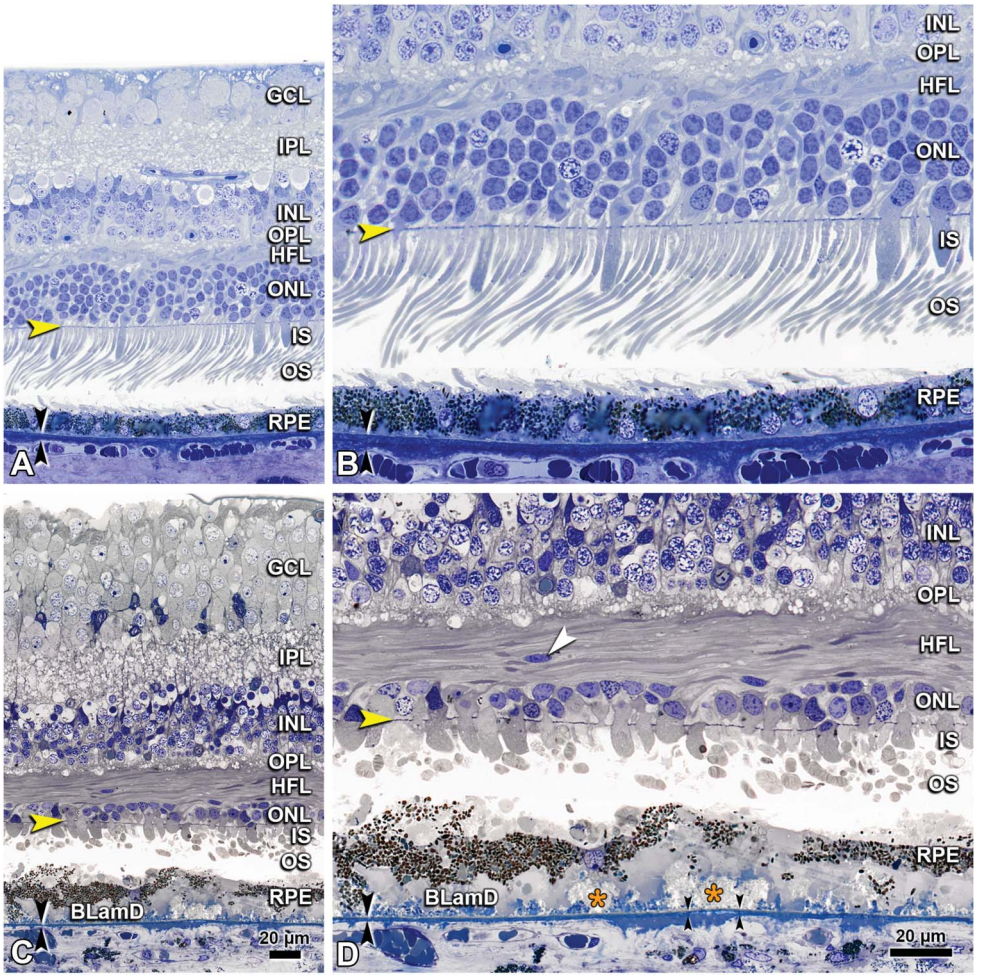

Fig. 4. Thinning of outer nuclear layer in eyes with geographic atrophy. GCL, ganglion cell layer; IPL inner plexiform layer; INL, inner nuclear layer; external limiting membrane, yellow arrowheads; IS, inner segment; OS, outer segment; Bruch membrane, black arrowheads. Bar in (**C**) applies to (**A**) and (**C**); bar in (**D**) applies to (**B**) and (**D**). **A** and **B.** Outer nuclear layer in the central section is unremarkable, where more than four layers of photoreceptor nuclei are seen. Eighty-five-year-old woman. **C** and **D.** Outer nuclear layer in the central section is thin, with one to two layers of degenerative photoreceptor nuclei remained. Photoreceptor nucleus ectopic to HFL, white arrowhead in (**D**); Bruch membrane calcification, small black arrowheads in (**D**). Basal mounds, orange asterisks. Eighty-three-year-old woman.

(disordered and absent) increased from 28.6% to 84%. Unremarkable and thinned ONL (Figure 4) decreased from 34.3% and 28.6% of locations, respectively, in the non-atrophic area to zero in the atrophic area, while ORT/island and absent ONL (Figure 6) increased from zero to 16.0% and 84.0% of locations respectively in the atrophic zone (Table 1). Retracted nuclei/mitochondria and dyslaminated HFL/ONL (Figure 5) are common (45.2% and 40.3%, respectively, of locations at −100 μm).

The distance between the OPL and ELM thinned significantly towards atrophic areas (P = 0.0380) but

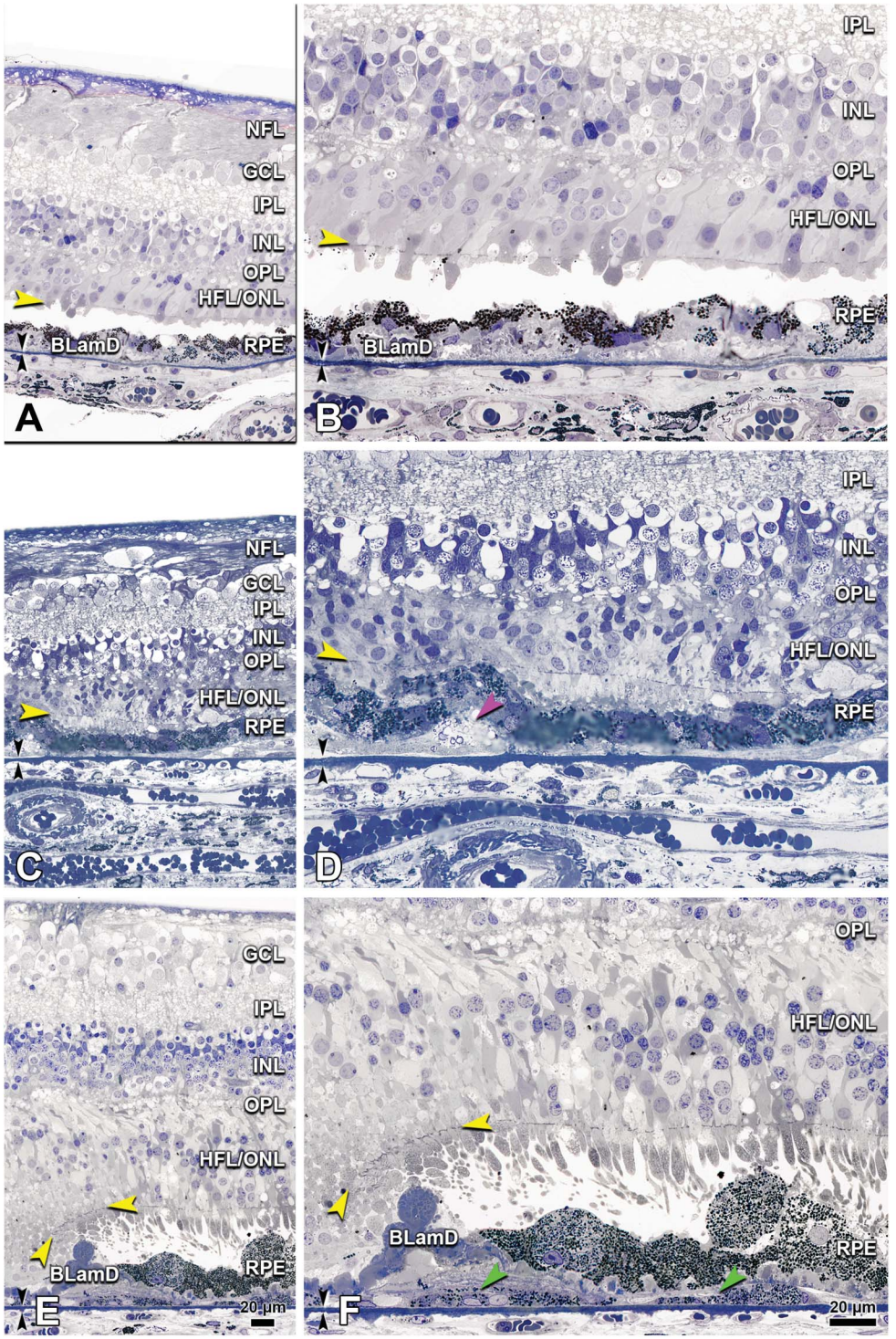

Fig. 5. Henle fiber layer and outer nuclear layer dyslamination in eyes with geographic atrophy. NFL, nerve fiber layer; GCL, ganglion cell layer; IPL inner plexiform layer; INL, inner nuclear layer; external limiting membrane (ELM), yellow arrowheads; IS, inner segment; OS, outer segment; Bruch membrane, black arrowheads. Bar in (**E**) applies to (**A**), (**C**) and (**E**); bar in (**F**) applies to (**B**), (**D**) and (**F**). **A** and **B.** Dyslamination of HFL and ONL in the superior perifovea (200 μm to ELM descent, non-atrophic side), which photoreceptor nuclei scattered into HFL and the boundary between HFL and ONL is not visible. Eighty-five-year-old woman. **C** and **D.** Dyslamination of HFL and ONL in the superior perifovea (at the border of ELM descent, non-atrophic side). Calcified drusen, pink arrowheads. Eighty-eight-year-old woman. **E** and **F.** Dyslamination of HFL and ONL at the central section (at the ELM descent, non-atrophic side). Subducted RPE cells, green arrowheads. Eighty-seven-year-old man.

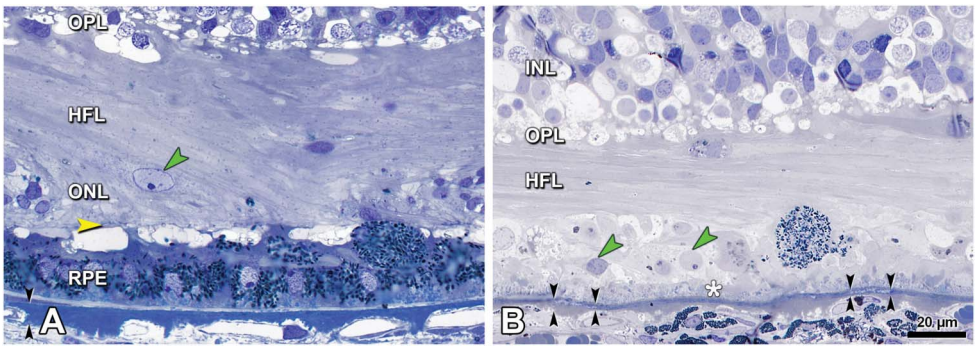

Fig. 6. Atrophy of outer nuclear layer in geographic atrophy. **A.** Meets the criterion for complete outer retinal atrophy (cORA) and (**B**), for complete RPE and outer retinal atrophy (cRORA).[10] INL, inner nuclear layer; external limiting membrane (ELM), yellow arrowhead; RPE, retinal pigment epithelium; Bruch membrane, black arrowheads. Bar in (**B**) applies to (**A**) and (**B**). **A.** RPE is intact but HFL consists of Müller cells only and ONL is atrophic. ELM is visible (yellow arrowhead) as is the nucleus of a presumed degenerating photoreceptor (green arrowhead). Eighty-eight-year-old woman. **B.** Cone photoreceptor nuclei (green arrowheads) are present but do not form a continuous layer. ELM is not visible. BLamD is discontinuous (white asterisk). Bruch membrane calcification, black arrowheads. Eighty-five-year-old woman.

remained substantial, even within the atrophic zone (48.9 μm at +100 μm vs. 27.2 μm at +500 μm) (Table 1). In contrast, ONL thickness decreased from 27.9 μm to 0 μm ($P = 0.0094$), and rows of ONL decreased from 3 to 0, crossing from the non-atrophic to the atrophic area. Accordingly, the proportion of ONL to OPL-ELM thickness decreased from 48.1% to 0% over this distance, because the combined HFL/ONL thickness was accounted for almost exclusively by Müller glia, which can be considered an endpoint of the gliotic process. Inner segment myoid was significantly thicker on the non-atrophic side (pooled −100 and −500 μm) than the atrophic side (pooled +100 and +500 μm) (2.3 ± 2.8 μm vs. 0.0 ± 0.0 μm, $P <$ 0.0391).

Ectopic RPE cells refer to previously described intra-retinal RPE.[9,31] Isolated melanosome/lipofuscin (M/L) granules (Figure 7B) or those associated with ectopic RPE cell bodies were assessed together as pigment migration to outer retina (Figure 7A). As summarized in Table 2, pigment migration was less common on the non-atrophic side of the ELM descent (37.1% and 22.9%) than on the atrophic side (70.3% and 44.0% of locations at +100 and +500 μm, respectively).

Thicknesses of the RBB and adjoining sub-retinal compartment are shown in Table 3. Subretinal drusenoid deposit thickness declined from 2.8 ± 3.9 μm at −500 μm to 0.0 ± 0.0 μm at +500 μm, $P = 0.0493$. Retinal pigment epithelium thickened from 12.1 ± 5.2 μm to 14.5 ± 7.2 in the non-atrophic side of the ELM descent and declined to 0.2 ± 1.2 μm and 0.0 ± 0.0 μm in the atrophic side ($P = 0.0179$). Thickness of RPE + BLamD parallels the trend in the RPE layer, that is, 19.3 ± 8.2 μm, 22.6 ± 11.1 μm, 7.7 ± 5.9 μm, and 5.1 ± 7.0 μm across the ELM descent landmark ($P = 0.0296$). Thicknesses of other single and combined layers in Table 3 did not vary significantly across this boundary.

By histology, ChC degeneration can be divided into five stages, in relation to a "Roman arch bridge" created by the deeply stained intercapillary pillars of BrM outer collagenous layer: unremarkable (Figure 8A), retracted endothelium[37] (Figure 8B), ghost (absent endothelium) with cells filling the arch (Figure 8C), ghost without cells (Figure 8C), and de-pillared (Figure 8D). ChC is considered retracted if endothelium occupies less than 50% of the space between the adjacent pillars. Various cells can present in the space vacated by ChC (see **Figure, Supplemental Digital Content 1**, http://links.lww.com/IAE/A855). We counted as "ghost with cells" only those with heterogeneous inclusions consistent with phagocytes. De-pillared ChC is the end stage, in which intercapillary pillars disappear, leaving BrM as a straight, blue-stained line.

Unremarkable ChC (Table 4, and Figure 8 A1 and A2) decreased from 58.3% of locations in the non-atrophic side of the ELM descent to 12.0% in the atrophic area, while de-pillared ChC (Figure 8 D1 and D2) increased from 0.0% of locations on the non-atrophic side (−500 μm) to 20.0% on the atrophic side (+500 μm). Retracted ChC (Figure 8 B1 and B2) was most frequently seen at −100 μm (29.0% of locations). Ghosts with cells (28.0%) and ghosts (30.4%) were common at +500 and +100 μm, respectively (Figure 8 C1 and C2). ChC density decreased significantly from 0.45 ± 0.17 at −500 μm to 0.21 ± 0.15 at +500 μm ($P = 0.0474$, Table 5). Bruch membrane was significantly thicker (1.79 ± 0.46 μm vs. 1.55 ± 0.43 μm, $P = 0.0446$, Table 5) on the non-atrophic side (pooled −100 and −500 μm) than on the atrophic side (pooled +100 and +500 μm).

We compared gradients of decreasing ONL thickness to status of the supporting tissues (Table 6). Reactive ($P = 0.0036$) and absent ($P < 0.0001$) RPE morphologies were more likely to be associated

Table 1. Outer Retinal Cellular and Laminar Phenotypes and Thicknesses (170 Locations)

Distance to ELM Descent, μm	−500	Non-Atrophic	−100	ELM Descent	+100	Atrophic	+500	*P*
Ectopic photoreceptor nuclei, % of locations								
No ectopic nuclei	8.6		6.5		78.7		72.0	—
Ectopic nuclei in IS	11.4		9.7		0.0		0.0	—
Ectopic nuclei in OPL/HFL	62.9		48.4		0.0		0.0	—
Absent OPL/HFL/ONL or dyslamination	20.0		38.7		21.3		28.0	—
HFL/ONL phenotypes*, % of locations								
Ordered HFL	57.1		41.9		27.7		16.0	—
Disordered HFL	22.9		17.7		53.2		60.0	—
Absent HFL	5.7		0.0		4.3		24.0	—
Unremarkable ONL	34.3		1.6		0.0		0.0	—
Thinned ONL	28.6		3.2		0.0		0.0	—
Retracted nuclei & mitochondria	22.9		45.2		17.0		0.0	—
Dyslaminated HFL/ONL	14.3		40.3		14.9		0.0	—
ORT/island	0.0		4.8		4.3		16.0	—
Absent ONL	0.0		4.8		63.8		84.0	—
HFL/ONL/ISmy thicknesses, μm								
OPL-ELM thickness	56.7 ± 22.1		51.1 ± 22.1		48.9 ± 32.6		27.2 ± 18.7	**0.0380**
ONL thickness†	27.9 ± 12.2		23.4 ± 12.9		0.0 ± 0.0		0.0 ± 0.0	**0.0094**
ONL to OPL-ELM proportion, %	48.1 ± 15.0		42.7 ± 15.0		0.0 ± 0.0		0.0 ± 0.0	—
ONL rows† (Median, IQR)	3, 1.8		3, 1.0		0, 0		0, 0	—
ISmy thickness‡	3.6 ± 3.2		1.5 ± 2.3		0.0 ± 0.0		NA	§**0.0391**

Ordered HFL, disordered HFL, absent HFL, and dyslaminated HFL/ONL add up to 100%; Unremarkable ONL, thinned ONL, retracted nuclei & mitochondria, dyslaminated HFL/ONL, ORT/island and absent ONL add up to 100%.

Generalized estimating equations linear model is used to compare mean OPL-ELM thickness, ONL thickness, ISmy thickness by assessment locations; and GEE logistic regression is used to compare presence or absence of ONL rows by assessment locations.

P value in bold <0.05.

*For HFL/ONL phenotypes at −500 μm from ELM descent, n = 35, one location was not included because the retina is missing.

†When ONL formed an ORT/island,[22] retracted nuclei and mitochondria, or is dyslaminated, the values of ONL thickness and ONL rows are recorded as not available.

‡When ISmy belongs to an ORT/island,[22] or no IS because of complete PR atrophy, the value of ISmy thickness is recorded as not available.

§Comparison of ISmy thickness is done between non-atrophic (pooled −100 and −500 μm) and atrophic (pooled +100 and +500 μm) area, while OPL-ELM thickness and ONL thickness are compared among 4 different locations (−500, −100, +100 and +500 μm).

IS, inner segment; IQR, interquartile range; my, myoid.

Table 2. Ectopic RPE Cells and/or Melanosome/Lipofuscin Granules in Outer Retina (170 Locations)

Ectopic RPE Cell and/or M/L Granules (% of Locations)	Distance to ELM Descent, μm: −500*	Non-Atrophic	−100	ELM Descent	+100	Atrophic	+500
No RPE cells or M/L granules	77.1		62.9		25.5		36.0
RPE cells and/or M/L granules presence	22.9		37.1		72.4		44.0
RPE cells and/or M/L granules in OPL/HFL and/or ONL	22.9		16.1		57.5		44.0
RPE cells and/or M/L granules in dyslaminated OPL/HFL-ONL	0.0		21.0		12.8		0.0
Absent OPL/HFL/ONL	0.0		0.0		4.3		20.0

*N = 35 at location −500, one location was not included because the retina is missing.

M/L, melanosome/lipofuscin.

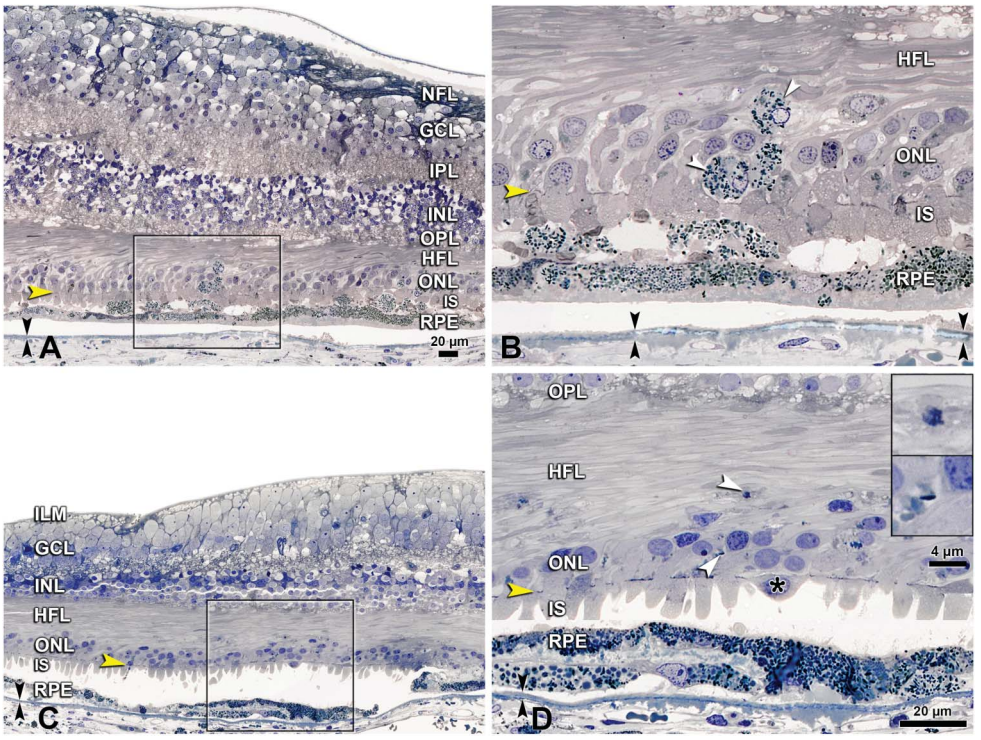

Fig. 7. Pigment migration to outer nuclear layer and Henle fiber layer in eyes with geographic atrophy. ILM, inner limiting membrane; GCL, ganglion cell layer; IPL, inner plexiform layer; INL, inner nuclear layer; external limiting membrane, yellow arrowheads; IS, inner segment; OS, outer segment; Bruch membrane, black arrowheads. Bar in (**C**) applies to (**A**) and (**C**); bar in (**D**) applies to (**B**) and (**D**). **A** and **B.** RPE cells (white arrowheads in B) migrated to ONL and HFL. Bruch membrane calcification, black arrowheads in (B). Eighty-six-year-old woman. **C** and **D.** Melanosomes (white arrowheads and insets in D) migrated to ONL and HFL. Photoreceptor nucleus ectopic to IS, black asterisk in (**D**). Eighty-eight-year-old woman.

with complete ONL atrophy (i.e., ONL thickness = 0 μm), compared to normal RPE morphology. Complete ONL atrophy was associated with thinner RBB (due to loss of RPE; 30.58 ± 19.60 μm vs. 18.60 ± 21.72 μm, $P = 0.001$), thinner BrM (1.53 ± 0.41 μm vs. 1.76 ± 0.44 μm, $P = 0.0067$), and lower ChC density (0.23 ± 0.18 vs. 0.42 ± 0.19, $P < 0.0001$) than non-atrophic ONL (i.e., ONL thickness >0 μm). Of layers tested, only RPE morphology was related to dyslaminated ONL, as absent ($P = 0.0142$) and reactive RPE ($P = 0.0557$, borderline significance) were more likely to associate with ONL dyslamination than normal RPE.

Discussion

Long focused on RPE atrophy via color fundus photography and then FAF, GA is being redefined as cRORA to incorporate retinal pathology revealed by OCT.[3,10] To clarify underlying pathologic mechanisms of GA, inform OCT interpretation, and investigate new biomarkers, we analyzed photoreceptor atrophy and gliosis relative to the ELM descent and to underlying supporting tissues. Our findings include: 1) ELM descent is a sharp border of photoreceptor and RPE atrophy in GA. 2) In the atrophic area a continuous layer of photoreceptors with inner and outer

Table 3. Subretinal Drusenoid Deposit, RPE, BLamD and Sub-RPE-BL Thickness (170 Locations)

Distance to ELM Descent, μm	−500	−100	+100	+500	*P*
	Non-Atrophic		ELM Descent	Atrophic	
SDD, μm	2.8 ± 3.9	1.4 ± 3.0	0.0 ± 0.0	0.0 ± 0.0	**0.0493**
RPE, μm	12.1 ± 5.2	14.5 ± 7.2	0.2 ± 1.2	0.0 ± 0.0	**0.0179**
BLamD, μm	7.2 ± 6.1	8.1 ± 8.1	7.5 ± 5.6	5.1 ± 7.0	0.4279
Sub-RPE-BL, μm	5.6 ± 10.6	6.6 ± 13.6	8.7 ± 17.3	8.1 ± 13.1	0.5971
RPE + BLamD, μm	19.3 ± 8.2	22.6 ± 11.1	7.7 ± 5.9	5.1 ± 7.0	**0.0296**
SDD + RPE + BLamD + sub-RPE-BL, μm	27.6 ± 14.3	29.9 ± 18.4	15.5 ± 17.2	12.6 ± 19.2	0.0638

Generalized estimating equations linear model is used to compare mean SDD, RPE, BLamD, sub-RPE-BL, RPE + BLamD and SDD + RPE + BLamD + sub-RPE-BL thicknesses by assessment locations.

P value in bold <0.05. Comparisons were conducted among the four different locations.

SDD, subretinal drusenoid deposit; sub-RPE-BL, sub-RPE-basal laminar.

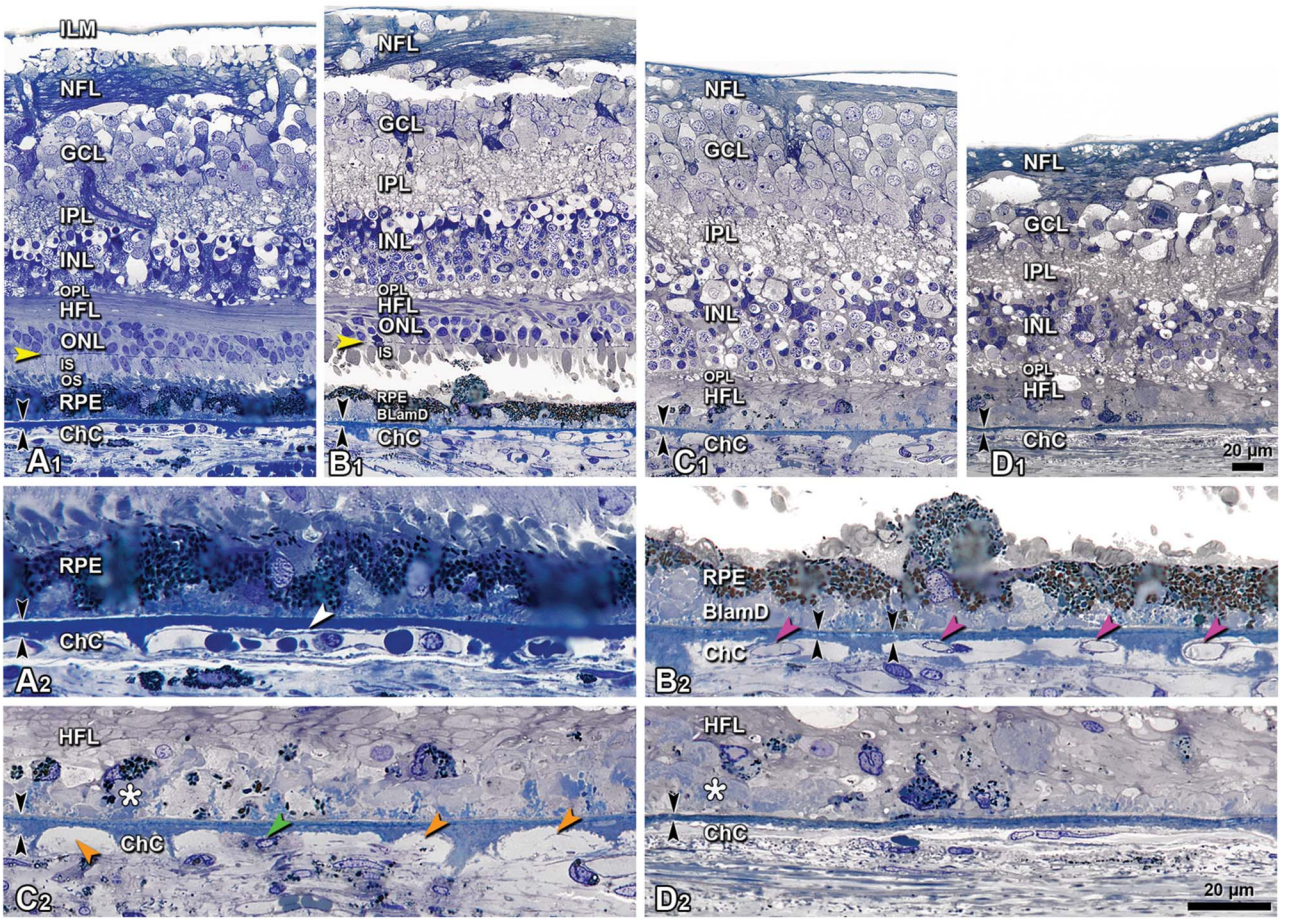

Fig. 8. Five stages of choriocapillaris degeneration in eyes with geographic atrophy. ILM, inner limiting membrane; GCL, ganglion cell layer; IPL, inner plexiform layer; INL, inner nuclear layer; external limiting membrane, yellow arrowheads; IS, inner segment; OS, outer segment; RPE, retinal pigment epithelium; Bruch membrane, black arrowheads. Bar in (**G**) applies to (**A**), (**C**), (**E**) and (**G**); bar in (**H**) applies to (**B**) (**D**) (**F**) and (**H**). **A1** and **A2.** The ChC, which fully occupies the arches of Bruch membrane, is unremarkable. Blood cells are detectable within the vessel. Eighty-eight-year-old woman. **B1** and **B2.** The ChC are retracted (pink arrowheads), which fill up less than 50% of the area between two intercapillary pillars of Bruch membrane. Bruch membrane calcification, black arrowheads in (D). Eighty-three-year-old woman. **C1** and **C2.** Ghost ChC (orange arrowheads), of which the endothelium are gone/fading, and a ghost ChC with a macrophage (green arrowhead) are detected. Basal laminar deposit is discontinuous (white asterisk). Eighty-three-year-old woman. **D1** and **D2.** ChC in the de-pillared stage, where the intercapillary pillars of Bruch membrane have disappeared, as well as the endothelia and phagocytes. Basal laminar deposit is discontinuous (white asterisk). Eighty-three-year-old woman.

segments is absent, and the remaining HFL is comprised of Müller cell processes. 3) In contrast to the retina, BrM and ChC density show gradual and monotonic degenerative changes, and BLamD and sub-RPE-BL thickness show no significant change, from the non-atrophic to the atrophic sides, across the ELM descent. Our results suggest that the distinct GA border in the retina may be due to massive protective responses by Müller cells reaching a threshold to the gradual decline of the underlying supporting tissues.

Table 4. Stages of Choriocapillaris Degeneration (170 Locations)

	Distance to ELM Descent, μm				
	−500	−100		+100	+500
ChC Degeneration (% of Locations)	Non-atrophic		ELM descent		Atrophic
Unremarkable	58.3	35.5		23.9	12.0
Retracted	25.0	29.0		15.2	24.0
Ghost with cells	5.6	17.7		15.2	28.0
Ghost	11.1	14.5		30.4	16.0
De-pillared	0.0	3.2		15.2	20.0

Table 5. Bruch Membrane Thickness and Choriocapillaris Density (170 Locations)

Distance to ELM Descent, μm	−500		−100		+100		+500	*P*
		Non-Atrophic		ELM Descent		Atrophic		
BrM thickness, μm	1.87 ± 0.48		1.75 ± 0.44		1.63 ± 0.43		1.41 ± 0.39	**0.0446***
ChC density	0.45 ± 0.17		0.38 ± 0.20		0.25 ± 0.15		0.21 ± 0.15	**0.0474**

Generalized estimating equations linear model is used to compare mean BrM thickness and ChC density by assessment locations.
P value in bold <0.05.
*Comparison of BrM thickness was done between non-atrophic (pooled −100 and −500 μm) and atrophic (pooled +100 and +500 μm) area, while ChC density was compared among 4 different locations (−500, −100, +100 and +500 μm).

Methodologic Considerations

Our report advances the histopathology literature on GA[37,47–49] with analytic approaches grounded in stereology and morphometry.[9,27,35,50,51] To discretize continuous variation in morphology and location, we used unbiased systematic sampling, vertical line probes crossing layers, and a cellular phenotyping system. We specified locations relative to a precise and biologically relevant border of GA lesions, the ELM descent. In our analysis, the progression of retinal changes in space from non-atrophic to atrophic sides implies a progression in time that may be related to the pathogenesis of the disease. Our visualization technique reveals all AMD-relevant layers in a single histologic section, subject to the constraints of retinal detachment, so we can address questions about the precedence of different tissue changes as the disease progresses.

Photoreceptor Degeneration and Gliosis

Our results contrast with prior histological studies that suggested less severe photoreceptor depletion in GA eyes. Kim et al[49] counted cells (n = 10 eyes) relative to the fovea (vs. relative to GA border) and did not report an area lacking photoreceptors. Bird et al[47] observed (n = 38 eyes) scattered cone cell bodies inside the GA area lacking continuous RPE and degenerating photoreceptors outside this area but did not report quantitative data. Eandi et al[48] described specimens (n = 15 eyes) as "missing RPE and thinned photoreceptor cell layer," that is, not implying or illustrating an area with absence of photoreceptors.

Normally highly compartmentalized, photoreceptors undergo significant subcellular reorganization in advanced AMD. Our recent studies of ORT[8,44–46,52] revealed longer survival of cones than rods, inward retraction of cone cell bodies from the ELM, and fissioning and translocation of mitochondria from cone inner segment ellipsoids towards cell bodies, resulting in shorter ISmy. Herein we further demonstrate that on the non-atrophic side of the GA border defined by the ELM descent, retracted nuclei and translocated mitochondria are predominant phenotypes (22.9% and 45.2% at −500 and −100 μm, respectively), consistent with numerous apoptotic photoreceptors previously seen near this border.[53] In our sample, ORTs were present at 16.0% of far-atrophic locations (+500 μm).

Table 6. Relationship of Outer Nuclear Layer Thickness to Status of Supporting System (170 Locations)

Locations With Different ONL Thicknesses (% of Locations)	>0	=0	*P**	Dyslaminated	*P**
RPE morphology					
Normal†	54.0	1.9	—	27.0	—
Reactive‡	44.4	35.8	**0.0036**	56.8	0.0557
Absent§	1.6	62.3	**<0.0001**	16.2	**0.0142**
Layer properties					
RBB thickness, μm¶	30.58 ± 19.60	18.60 ± 21.72	**0.0010**	29.70 ± 12.89	0.6667
BrM thickness, μm	1.76 ± 0.44	1.53 ± 0.41	**0.0067**	1.90 ± 0.45	0.1321
ChC density	0.42 ± 0.19	0.23 ± 0.18	**<0.0001**	0.36 ± 0.17	0.1549

P value in bold <0.05.
*A generalized logit model was used to assess the relationship between RPE morphology, RBB thickness, BrM thickness, and ChC density with ONL status.
†"Normal" includes uniform, non-uniform, and very non-uniform.
‡"Reactive" includes sloughed, shedding, bilaminar, intraretinal, and dissociated.
§"Absent" includes atrophy with BLamD and atrophy without BLamD.
¶"RBB thickness" = SDD + RPE + BLamD + sub-RPE-BL + BrM thickness.
RBB, RPE-basal lamina (BL)- Bruch membrane.

For the first time, we describe HFL/ONL dyslamination, a phenotype commonly found near the ELM descent, using terminology borrowed from brain pathology.[54] Numerous photoreceptor nuclei are found even in intact HFL (Figure 3), suggesting that this migration represents an early indicator of cellular stress. The HFL is distinct from ONL within a thick hyporeflective band of OCT,[13,14] and it can be intermittently reflective in normal and diseased eyes.[55] Whether these reflective signatures signify dyslamination, HFL disorder, or ectopic photoreceptor nuclei requires further clarification from direct clinicopathologic correlation in future studies. Single melanosomes within the HFL (Figure 7D) are likely carried by Müller cells, in contrast to fully nucleated RPE cells that could migrate autonomously. Finally, the atrophic HFL contains phagocytes, likely microglia migrated from inner retina.[56]

Our data further document the prodigious activity of Müller cells, coordinated with RPE degeneration, in GA. Müller cells bend laterally to form the ELM descent, and they outlast photoreceptors in end-stage ORT.[46,57] Here we show that they also outlast photoreceptors in the GA area, accounting for the entire OPL-ELM thickness when the ONL degenerates. Early studies[19,20] and recently, Edwards et al[58] reported Müller cells immunoreactive for glial fibrillary acidic protein in HFL/ONL of atrophic areas. In experimental retinal detachment,[59] Müller cell bodies reposition outwardly while remaining attached to the inner limiting membrane. They undergo mitosis and contribute to subretinal glial scars, a gliotic progression[18] that Edwards et al proposes also occurs in GA.[58] In the atrophic HFL we also saw dark-staining nuclei consistent with re-positioned Müller cells (see **Figure, Supplemental Digital Content 2**, http://links.lww.com/IAE/A856). Our histology reveals persistent BLamD, which separates subretinal and sub-RPE compartments in the absence of RPE.[39,60] Thus we see many Müller cells processes within the sub-RPE-BL space, likely attempting to clear drusen. Persistent BLamD is seen clinically as a moderately hyperreflective line extending across atrophic areas, either as a series of undulations (outer retinal corrugations)[15] or a single elevated line (plateau).[16] A fine punctate reflectivity external to this line when elevated likely represents Müller cells. Basal laminar deposit also persists as an irregular line directly opposed to BrM.

Gliosis of Müller cells in retinal disease can be both protective and detrimental.[61,62] Protective effects include phagocytosis of exogenous substances and cellular debris,[61] and also release of antioxidants and neurotrophic factors.[61] Indeed, Müller cells scrolling cones into ORT can be viewed as protection from the failing RBB,[46,63,64] or from factors released by dying cells in the atrophic area. However, this level of gliosis indicates very advanced disease stage, when therapeutic interventions are less likely to be successful. Glial scars may represent attempted restoration of barrier functions normally served by the ELM; they may also complicate the therapeutic transplantation of cells.[58]

Interpretation of Optical Coherence Tomography and Other Diagnostic Technologies

Histology can suggest metrics for clinical studies involving OCT-based endpoints for GA, with careful interpretation. The ELM descent delimits the atrophic area, from which the ELM is absent, and represents a distinct border for the GA lesion. The measurement of the total distance between OPL and ELM avoids potential effects of dyslamination on HFL/ONL visibility, but cannot be used to assess photoreceptor abundance or outer retinal integrity,[65] because it may consist of only Müller cells in eyes with severe gliosis (Figure 6). Inner segment myoid, a hyporeflective band between ELM and EZ, shrinks due to inward mitochondrial translocation[8]; the EZ band itself may disappear $<500\ \mu$m from the actual GA border. Due to artifacts common in donor eyes, we could not obtain reliable histological data on all photoreceptor parts contributing to outer retinal reflective bands. However, from ISmy changes, we can infer disintegrity and loss of EZ, which has been reported clinically.[66]

We relate our results to OCT studies of Müller glia and photoreceptors in GA. A hyporeflective wedge within HFL often appears on the atrophic side of the GA border.[67] Increased reflectivity of HFL/ONL, perhaps due to gliosis, is suggested as a predictor of GA enlargement.[68] Reactive Müller cells are invoked to explain ONL thickening[69,70] and lifting of persistent BLamD off BrM.[15,16] The curving ELM descent[71] and ELM disruption or breakage[72–76] is visible. A reduction in EZ reflectivity that predicts the direction of GA progression[77,78] can be related to a thickened RBB in these areas (Table 6). Another sign of photoreceptor degeneration is OPL subsidence,[79] but some descriptions ("thinned and shifted)"[80,81] and illustrations[82] resemble persistent BLamD, so more data are needed.

Our data are relevant to other technologies probing photoreceptors, in addition to OCT. Adaptive optics scanning laser ophthalmoscopy reveals reflections from individual cones viewed *en face*.[40,41] Decreased cone reflectance at the GA border is consistent with our observations of photoreceptor degeneration that could degrade wave guiding. Inconsistent adaptive optics scanning laser ophthalmoscopy findings on cone spatial density[83,84] are not addressed by our data.

However, our current and past[47,48] studies together suggest that the quasi-regular reflective puncta seen by adaptive optics scanning laser ophthalmoscopy within the GA area[52,83,84] represent processes of activated Müller cells and possibly phagocytes. Our data are also relevant to microperimetry, which tests visual function at photopic and mesopic levels of illumination.[85] In patients with GA, absolute scotoma in the atrophic area[86] expands and initially relative scotomas convert to absolute scotoma over time.[73,75,87,88] Sensitivities to stimuli placed directly on GA borders are poorer than they are just 500 μm away,[89] consistent with our assessment. Poor sensitivities associate with EZ disintegrity,[90,91] RPE thickening and hyperautofluorescence,[91] and by inference, HFL/ONL dyslamination. Thus, loss of visual function in GA involves highly local phenomena.

Status of the Photoreceptor Supporting System

For the first time, we describe de-pillarization, a manifestation of advanced ChC degeneration. Choriocapillaris endothelium appears required for maintaining not only its own basal lamina but also the outer collagenous layer of BrM. For this reason, BrM is significantly thinner in the atrophic side than the non-atrophic side of GA, in alignment with some[37] but not other previous reports.[29,47] Our analysis used a three-layer definition of BrM[92,93] (inner and outer collagenous layers plus elastic layer) that does not include the RPE and ChC basal laminas, as advised by Gass and Sarks.[90,91] Thus extracellular deposits were included in sub-RPE thickness measurements,[94] whereas Bird et al[47] who reported BrM thickening in the GA area, included BLamD with BrM. We found that BLamD does not thin across the ELM descent (Table 3).

Across the ELM descent, from non-atrophic to atrophic sides of the GA border, we showed both a gradual increase of pathologic ChC phenotypes (Table 4) and decrease of ChC density (Table 5). The latter is a metric of metabolic exchange capacity. Our measured values (0.45–0.38 non-atrophic side vs. 0.25–0.21 atrophic side) are at the low end of the published range for non-atrophic versus atrophic areas,[27,29,37,95,96] and concur with a steady decline across the GA border seen previously.[95] Collectively, these data support the interpretation of OCT angiography, a technique that detects optical reflectivity from moving cells in vasculature.[97] Flow signal at the level of the ChC is reportedly reduced, but not to zero, within GA,[97–99] and may also be reduced,[100,101] to a lesser degree, in surrounding non-atrophic areas, both consistent with our data.

Timeline of Degeneration Across Tissues

The gradual deterioration of BrM and ChC across the ELM descent reflects lifelong processes documented for both tissues[24,28,29,102] that culminate in drusen in the sub-RPE-BL space in early and intermediate AMD.[103] The spatial characteristics of BrM and ChC change contrast markedly with a degenerative transition involving first the RPE[104,105] then photoreceptors and Müller cells, as encapsulated by the ELM descent. The latter are more logically a cellular response to BrM-ChC events that reach some threshold of stress than the other way around. One possible stressor is increased diffusion distance of RPE from ChC caused by accumulation of BLamD and drusen.[31] Another is accumulation of pro-inflammatory and cytotoxic lipids in drusen.[106] The concept that AMD is fundamentally a vascular-metabolic disease rather than a primary neurodegeneration is supported by the finding that impairment of dark adaptation, a visual test that is rate-limited by retinoid supply across the RPE-BrM-ChC interface, is the first functional abnormality in clinically incipient AMD.[107,108] Other authors considered whether RPE and ChC are affected first in AMD pathogenesis.[27,37,95,96,109] Bruch membrane plays a central role, since its age-related lipid accumulation begins early in the aging process and can be experimentally re-created[103] in a manner consistent with clinical observations of druse dynamism.[110,111] A better understanding of triggering factors and the sequence of events in AMD progression is key to directing therapeutic strategies towards GA precursors.[112,113]

Conclusion

Strengths of this study were the use of high-resolution comprehensive histopathology and photodocumentation and unbiased sampling methods to assess progression and clearing processes in multiple tissue layers. Limitations were the small number of eyes, post-mortem artifact which prevented assessing all contributors to photoreceptor-attributable bands, and lack of in vivo clinical histories. Nevertheless, our data offer a new perspective on the question of which layer exhibits initial changes in AMD by systematically sampling more layers across the outer retinal neurovascular unit than any previous study, clinical or histological. Data are expected to inform the interpretation of clinical multimodal imaging anchored on OCT, mechanistic studies of photoreceptor fate, and therapeutic strategies for AMD. Finally, our data encourage the identification of novel clinical trial endpoints, associated with earlier stages of AMD, ideally before irreversible tissue damage begins.

Key words: age-related macular degeneration, retina, photoreceptors, Müller cells, retinal pigment epithelium, choriocapillaris, Bruch membrane, geographic atrophy, histology, morphometry.

Acknowledgments

The authors thank the Alabama Eye Bank for timely retrieval of donor eyes, and David Fisher for drawings on Figure 2.

References

1. Wong WL, Su X, Li X, et al. Global prevalence of age-related macular degeneration and disease burden projection for 2020 and 2040: a systematic review and meta-analysis. Lancet Glob Health 2014;2:e106–e116.
2. Maguire MG, et al. Five-year outcomes with anti-vascular endothelial growth factor treatment of neovascular age-related macular degeneration: the comparison of age-related macular degeneration treatments trials. Ophthalmology 2016;123:1751–1761.
3. Holz FG, et al. Imaging protocols in clinical studies in advanced age-related macular degeneration: recommendations from classification of atrophy consensus meetings. Ophthalmology 2017;124:464–478.
4. Csaky KG, Richman EA, Ferris FL III. Report from the NEI/FDA ophthalmic clinical trial design and endpoints symposium. Invest Ophthalmol Vis Sci 2008;49:479–489.
5. CTGTAC Meeting #52. Cellular and Gene Therapies for Retinal Disorders. Vol 2016: FDA Cellular, Tissue, and Gene Therapies Advisory Committee; Silver Spring, MD: 2011.
6. Fleckenstein M, et al. The progression of geographic atrophy secondary to age-related macular degeneration. Ophthalmology 2018;125:369–390.
7. Drasdo N, et al. The length of Henle fibers in the human retina and a model of ganglion receptive field density in the visual field. Vis Res 2007;47:2901–2911.
8. Litts KM, et al. Inner segment remodeling and mitochondrial translocation in cone photoreceptors in age-related macular degeneration with outer retinal tubulation. Invest Ophthalmol Vis Sci 2015;56:2243–2253.
9. Zanzottera EC, et al. Visualizing retinal pigment epithelium phenotypes in the transition to geographic atrophy in age-related macular degeneration. Retina (Philadelphia, PA) 2016;36:S12–S25.
10. Sadda SR, et al. Consensus definition for atrophy associated with age-related macular degeneration on oct: classification of atrophy report 3. Ophthalmology 2018;125:537–548.
11. Spaide RF, Curcio CA. Anatomical correlates to the bands seen in the outer retina by optical coherence tomography: literature review and model. Retina (Philadelphia, PA) 2011;31:1609–1619.
12. Staurenghi G, et al. Proposed lexicon for anatomic landmarks in normal posterior segment spectral-domain optical coherence tomography: the IN*OCT consensus. Ophthalmology 2014;121:1572–1578.
13. Curcio CA, et al. Human chorioretinal layer thicknesses measured in macula-wide, high-resolution histologic sections. Invest Ophthalmol Vis Sci 2011;52:3943–3954.
14. Lujan BJ et al. Revealing Henle's fiber layer using spectral domain optical coherence tomography. Invest Ophthalmol Vis Sci 2011;52:1486–1492.
15. Ooto S, et al. Outer retinal corrugations in age-related macular degeneration. JAMA Ophthalmol 2014;132:806–813.
16. Tan ACS, et al. The evolution of the plateau, an optical coherence tomography signature seen in geographic atrophy. Invest Ophthalmol Vis Sci 2017;58:2349–2358.
17. Sarks SH. Ageing and degeneration in the macular region: a clinico-pathological study. Br J Ophthalmol 1976;60:324–341.
18. Bringmann A, Wiedemann P. Muller glial cells in retinal disease. Ophthalmologica 2012;227:1–19.
19. Guidry C, Medeiros NE, Curcio CA. Phenotypic variation of retinal pigment epithelium in age-related macular degeneration. Invest Ophthalmol Vis Sci 2002;43:267–273.
20. Wu KH, et al. Differential expression of GFAP in early v late AMD: a quantitative analysis. Br J Ophthalmol 2003;87:1159–1166.
21. Chen W, et al. Choroidal and photoreceptor layer thickness in myopic population. Eur J Ophthalmol 2012;22:590–597.
22. Hawkins BT, Davis TP. The blood-brain barrier/neurovascular unit in health and disease. Pharmacol Rev 2005;57:173–185.
23. Newman EA. Glial cell regulation of neuronal activity and blood flow in the retina by release of gliotransmitters. Philos Trans R Soc Lond B Biol Sci 2015:370.
24. Curcio CA, et al. Accumulation of cholesterol with age in human Bruch's membrane. Invest Ophthalmol Vis Sci 2001;42:265–274.
25. Adhi M, et al. Characterization of choroidal layers in normal aging eyes using enface swept-source optical coherence tomography. PLoS One 2015;10:e0133080.
26. Ferrara D, Waheed NK, Duker JS. Investigating the choriocapillaris and choroidal vasculature with new optical coherence tomography technologies. Prog Retin Eye Res 2016;52:130–155.
27. Biesemeier A, et al. Choriocapillaris breakdown precedes retinal degeneration in age-related macular degeneration. Neurobiol Aging 2014;35:2562–2573.
28. Mullins RF, et al. The membrane attack complex in aging human choriocapillaris: relationship to macular degeneration and choroidal thinning. Am J Pathol 2014;184:3142–3153.
29. Ramrattan RS, et al. Morphometric analysis of Bruch's membrane, the choriocapillaris, and the choroid in aging. Invest Ophthalmol Vis Sci 1994;35:2857–2864.
30. Balaratnasingam C, et al. Clinical characteristics, choroidal neovascularization, and predictors of visual outcomes in acquired vitelliform lesions. Am J Ophthalmol 2016;172:28–38.
31. Curcio CA, et al. Activated retinal pigment epithelium, an optical coherence tomography biomarker for progression in age-related macular degeneration. Invest Ophthalmol Vis Sci 2017; 58:BIO211–BIO226.
32. Pang CE, et al. The onion sign in neovascular age-related macular degeneration represents cholesterol crystals. Ophthalmology 2015;122:2316–2326.
33. Zanzottera EC, et al. Subducted and melanotic cells in advanced age-related macular degeneration are derived from retinal pigment epithelium. Invest Ophthalmol Vis Sci 2015;56:3269–3278.
34. Zanzottera EC, et al. The project macula retinal pigment epithelium grading system for histology and optical coherence tomography in age-related macular degeneration. Invest Ophthalmol Vis Sci 2015;56:3253–3268.
35. Curcio CA, et al. Subretinal drusenoid deposits in non-neovascular age-related macular degeneration: morphology,

prevalence, topography, and biogenesis model. Retina (Philadelphia, PA) 2013;33:265–276.
36. Curcio CA, et al. Correlation of type 1 neovascularization associated with acquired vitelliform lesion in the setting of age-related macular degeneration. Am J Ophthalmol 2015; 160:1024–1033.e1023.
37. Sarks JP, Sarks SH, Killingsworth MC. Evolution of geographic atrophy of the retinal pigment epithelium. Eye (London, England) 1988;2:552–577.
38. Vogt SD, et al. Retinal pigment epithelial expression of complement regulator CD46 is altered early in the course of geographic atrophy. Exp Eye Res 2011;93:413–423.
39. Zanzottera EC, et al. Visualizing retinal pigment epithelium phenotypes in the transition to atrophy in neovascular age-related macular degeneration. Retina (Philadelphia, PA) 2016; 36:S26–S39.
40. Polyak SL. The Retina. Chicago, IL: University of Chicago; 1941.
41. Perry VH, Cowey A. The lengths of the fibres of Henle in the retina of macaque monkeys: implications for vision. Neuroscience 1988;25:225–236.
42. Curcio CA, et al. Aging of the human photoreceptor mosaic: evidence for selective vulnerability of rods in central retina. Invest Ophthalmol Vis Sci 1993;34:3278–3296.
43. Burris C, et al. How Muller glial cells in macaque fovea coat and isolate the synaptic terminals of cone photoreceptors. J Comp Neurol 2002;453:100–111.
44. Litts KM, et al. Quantitative analysis of outer retinal tubulation in age-related macular degeneration from spectral-domain optical coherence tomography and histology. Invest Ophthalmol Vis Sci 2016;57:2647–2656.
45. Litts KM, et al. Clinicopathological correlation of outer retinal tubulation in age-related macular degeneration. JAMA Ophthalmol 2015;133:609–612.
46. Schaal KB, et al. Outer retinal tubulation in advanced age-related macular degeneration: optical coherence tomographic findings correspond to histology. Retina (Philadelphia, PA) 2015;35:1339–1350.
47. Bird AC, Phillips RL, Hageman GS. Geographic atrophy: a histopathological assessment. JAMA Ophthalmol 2014; 132:338–345.
48. Eandi CM, et al. Subretinal mononuclear phagocytes induce cone segment loss via IL-1beta. Elife 2016;5.
49. Kim SY, et al. Morphometric analysis of the macula in eyes with geographic atrophy due to age-related macular degeneration. Retina (Philadelphia, PA) 2002;22:464–470.
50. Curcio CA, Medeiros NE, Millican CL. Photoreceptor loss in age-related macular degeneration. Invest Ophthalmol Vis Sci 1996;37:1236–1249.
51. Curcio CA, et al. Peripapillary chorioretinal atrophy: bruch's membrane changes and photoreceptor loss. Ophthalmology 2000;107:334–343.
52. Litts KM, et al. Exploring photoreceptor reflectivity through multimodal imaging of outer retinal tubulation in advanced age-related macular degeneration. Retina (Philadelphia, PA) 2017;37:978–988.
53. Dunaief JL, et al. The role of apoptosis in age-related macular degeneration. Arch Ophthalmol 2002;120:1435–1442.
54. Reeves C, et al. Combined ex vivo 9.4T MRI and quantitative histopathological study in normal and pathological neocortical resections in focal epilepsy. Brain Pathol 2016;26:319–333.
55. Ouyang Y, et al. Different phenotypes of the appearance of the outer plexiform layer on optical coherence tomography. Graefes Arch Clin Exp Ophthalmol 2013;251:2311–2317.
56. Lad EM, et al. Abundance of infiltrating CD163+ cells in the retina of postmortem eyes with dry and neovascular age-related macular degeneration. Graefes Arch Clin Exp Ophthalmol 2015;253:1941–1945.
57. Dolz-Marco R, et al. The evolution of outer retinal tubulation, a neurodegeneration and gliosis prominent in macular diseases. Ophthalmology 2017;124:1353–1367.
58. Edwards MM et al. Subretinal glial membranes in eyes with geographic atrophy. Invest Ophthalmol Vis Sci 2017;58: 1352–1367.
59. Lewis GP, et al. The fate of Muller's glia following experimental retinal detachment: nuclear migration, cell division, and subretinal glial scar formation. Mol Vis 2010;16: 1361–1372.
60. Green WR, Enger C. Age-related macular degeneration histopathologic studies. The 1992 Lorenz E. Zimmerman Lecture. Ophthalmology 1993;100:1519–1535.
61. Bringmann A, et al. Cellular signaling and factors involved in Muller cell gliosis: neuroprotective and detrimental effects. Prog Retin Eye Res 2009;28:423–451.
62. Bringmann A, et al. Muller cells in the healthy and diseased retina. Prog Retin Eye Res 2006;25:397–424.
63. Anderson DH, et al. Morphological recovery in the reattached retina. Invest Ophthalmol Vis Sci 1986;27:168–183.
64. Erickson PA, et al. Glial fibrillary acidic protein increases in Muller cells after retinal detachment. Exp Eye Res 1987;44: 37–48.
65. Lujan BJ, et al. Directional optical coherence tomography provides accurate outer nuclear layer and Henle fiber layer measurements. Retina (Philadelphia, PA) 2015;35: 1511–1520.
66. Schmitz-Valckenberg S, et al. Optical coherence tomography and autofluorescence findings in areas with geographic atrophy due to age-related macular degeneration. Invest Ophthalmol Vis Sci 2011;52:1–6.
67. Mones J, Biarnes M, Trindade F. Hyporeflective wedge-shaped band in geographic atrophy secondary to age-related macular degeneration: an underreported finding. Ophthalmology 2012;119:1412–1419.
68. Stetson PF, et al. OCT minimum intensity as a predictor of geographic atrophy enlargement. Invest Ophthalmol Vis Sci 2014;55:792–800.
69. Schmitz-Valckenberg S, et al. In vivo imaging of foveal sparing in geographic atrophy secondary to age-related macular degeneration. Invest Ophthalmol Vis Sci 2009;50:3915–3921.
70. Ebneter A, et al. Relationship between presumptive inner nuclear layer thickness and geographic atrophy progression in age-related macular degeneration. Invest Ophthalmol Vis Sci 2016;57:OCT299–OCT306.
71. Fleckenstein M, et al. High-resolution spectral domain-OCT imaging in geographic atrophy associated with age-related macular degeneration. Invest Ophthalmol Vis Sci 2008;49: 4137–4144.
72. Fleckenstein M, et al. Tracking progression with spectral-domain optical coherence tomography in geographic atrophy caused by age-related macular degeneration. Invest Ophthalmol Vis Sci 2010;51:3846–3852.
73. Panorgias A, et al. Multimodal assessment of microscopic morphology and retinal function in patients with geographic atrophy. Invest Ophthalmol Vis Sci 2013;54:4372–4384.
74. Sadiq MA, et al. Structural characteristics of retinal layers adjacent to geographic atrophy. Ophthalmic Surg Lasers Imaging Retina 2015;46:914–919.

75. Wu Z, et al. Microperimetry of nascent geographic atrophy in age-related macular degeneration. Invest Ophthalmol Vis Sci 2014;56:115–121.
76. Wu Z, et al. Fundus autofluorescence characteristics of nascent geographic atrophy in age-related macular degeneration. Invest Ophthalmol Vis Sci 2015;56:1546–1552.
77. Niu S, et al. Fully automated prediction of geographic atrophy growth using quantitative spectral-domain optical coherence tomography biomarkers. Ophthalmology 2016;123:1737–1750.
78. Nunes RP, et al. Predicting the progression of geographic atrophy in age-related macular degeneration with SD-OCT en face imaging of the outer retina. Ophthalmic Surg Lasers Imaging Retina 2013;44:344–359.
79. Bearelly S, et al. Spectral domain optical coherence tomography imaging of geographic atrophy margins. Ophthalmology 2009;116:1762–1769.
80. Sayegh RG, et al. A systematic correlation of morphology and function using spectral domain optical coherence tomography and microperimetry in patients with geographic atrophy. Br J Ophthalmol 2014;98:1050–1055.
81. Sayegh RG, et al. A systematic comparison of spectral-domain optical coherence tomography and fundus autofluorescence in patients with geographic atrophy. Ophthalmology 2011;118:1844–1851.
82. Querques G, et al. Wedge-shaped subretinal hyporeflectivity in geographic atrophy. Retina (Philadelphia, PA) 2015;35:1735–1742.
83. Boretsky A, et al. In vivo imaging of photoreceptor disruption associated with age-related macular degeneration: a pilot study. Lasers Surg Med 2012;44:603–610.
84. Zayit-Soudry S, et al. Cone structure imaged with adaptive optics scanning laser ophthalmoscopy in eyes with nonneovascular age-related macular degeneration. Invest Ophthalmol Vis Sci 2013;54:7498–7509.
85. Hanout M, Horan N, Do DV. Introduction to microperimetry and its use in analysis of geographic atrophy in age-related macular degeneration. Curr Opin Ophthalmol 2015;26:149–156.
86. Hartmann KI, et al. Scanning laser ophthalmoscope imaging stabilized microperimetry in dry age-related macular degeneration. Retina (Philadelphia, PA) 2011;31:1323–1331.
87. Meleth AD, et al. Changes in retinal sensitivity in geographic atrophy progression as measured by microperimetry. Invest Ophthalmol Vis Sci 2011;52:1119–1126.
88. Pilotto E, et al. Short wavelength fundus autofluorescence versus near-infrared fundus autofluorescence, with microperimetric correspondence, in patients with geographic atrophy due to age-related macular degeneration. Br J Ophthalmol 2011;95:1140–1144.
89. Hariri AH, et al. Retinal sensitivity at the junctional zone of eyes with geographic atrophy due to age-related macular degeneration. Am J Ophthalmol 2016;168:122–128.
90. Pilotto E, et al. Microperimetry, fundus autofluorescence, and retinal layer changes in progressing geographic atrophy. Can J Ophthalmol 2013;48:386–393.
91. Takahashi A, et al. Photoreceptor damage and reduction of retinal sensitivity surrounding geographic atrophy in age-related macular degeneration. Am J Ophthalmol 2016;168:260–268.
92. Bressler SB, et al. Age-related macular degeneration: nonneovascular early AMD, intermediate AMD, and geographic atrophy. In: Ryan SJ, Schachat AP, eds. Retina. Philadelphia, PA: Elsevier Mosby; 2006:1041–1074.
93. Gass JDM. Stereoscopic Atlas of Macular Diseases: Diagnosis and Treatment. 4th ed. St. Louis, MO: Mosby; 1997.
94. Curcio CA, Johnson M. Structure, function, and pathology of Bruch's membrane. Retina (Philadelphia, PA) 2013;1:466–481.
95. McLeod DS, et al. Relationship between RPE and choriocapillaris in age-related macular degeneration. Invest Ophthalmol Vis Sci 2009;50:4982–4991.
96. Seddon JM, et al. Histopathological insights into choroidal vascular loss in clinically documented cases of age-related macular degeneration. JAMA Ophthalmol 2016;134:1272–1280.
97. Choi W, et al. Ultrahigh-speed, swept-source optical coherence tomography angiography in nonexudative age-related macular degeneration with geographic atrophy. Ophthalmology 2015;122:2532–2544.
98. Pellegrini M, et al. Dark atrophy: an optical coherence tomography angiography study. Ophthalmology 2016;123:1879–1886.
99. Moult EM, et al. Swept-source optical coherence tomography angiography reveals choriocapillaris alterations in eyes with nascent geographic atrophy and drusen-associated geographic atrophy. Retina (Philadelphia, PA) 2016;36:S2–S11.
100. Corbelli E, et al. Optical coherence tomography angiography in the evaluation of geographic atrophy area extension. Invest Ophthalmol Vis Sci 2017;58:5201–5208.
101. Kvanta A, et al. Optical coherence tomography angiography of the foveal microvasculature in geographic atrophy. Retina (Philadelphia, PA) 2017;37:936–942.
102. Huang JD, et al. Age-related changes in human macular Bruch's membrane as seen by quick-freeze/deep-etch. Exp Eye Res 2007;85:202–218.
103. Pilgrim MG, et al. Subretinal pigment epithelial deposition of drusen components including hydroxyapatite in a primary cell culture model. Invest Ophthalmol Vis Sci 2017;58:708–719.
104. Christenbury JG, et al. Progression of intermediate age-related macular degeneration with proliferation and inner retinal migration of hyperreflective foci. Ophthalmology 2013;120:1038–1045.
105. Ouyang Y, et al. Optical coherence tomography-based observation of the natural history of drusenoid lesion in eyes with dry age-related macular degeneration. Ophthalmology 2013;120:2656–2665.
106. Rodriguez IR, et al. 7-ketocholesterol accumulates in ocular tissues as a consequence of aging and is present in high levels in drusen. Exp Eye Res 2014;128:151–155.
107. Owsley C, et al. Delayed rod-mediated dark adaptation is a functional biomarker for incident early age-related macular degeneration. Ophthalmology 2016;123:344–351.
108. Steinmetz RL, et al. Symptomatic abnormalities of dark adaptation in patients with age-related Bruch's membrane change. Br J Ophthalmol 1993;77:549–554.
109. McLeod DS, et al. Quantifying changes in RPE and choroidal vasculature in eyes with age-related macular degeneration. Invest Ophthalmol Vis Sci 2002;43:1986–1993.
110. Balaratnasingam C, et al. Associations between retinal pigment epithelium and drusen volume changes during the lifecycle of large drusenoid pigment epithelial detachments. Invest Ophthalmol Vis Sci 2016;57:5479–5489.
111. Schlanitz FG, et al. Drusen volume development over time and its relevance to the course of age-related macular degeneration. Br J Ophthalmol 2017;101:198–203.
112. Vavvas DG, et al. Regression of some high-risk features of age-related macular degeneration (amd) in patients receiving intensive statin treatment. EBioMedicine 2016;5:198–203.
113. Rudolf M, et al. ApoA-I mimetic peptide 4F reduces age-related lipid deposition in murine Bruch's membrane and causes its structural remodeling. Curr Eye Res 2018;43:135–146.